

Nonlinear Robust Observers for State-of-Charge Estimation of Lithium-Ion Cells Based on a Reduced Electrochemical Model

Satadru Dey, Beshah Ayalew, and Pierluigi Pisu

Abstract—Advanced battery management systems rely on accurate cell- or module-level state-of-charge (SOC) information for effective control, monitoring, and diagnostics. Electrochemical models provide arguably the most accurate and detailed information about the SOC of lithium-ion cells. In this brief, two nonlinear observer designs are presented based on a reduced order electrochemical model. Both observers consist of a Luenberger term acting on nominal errors and a variable structure term for handling model uncertainty. Using Lyapunov’s direct method, the design of the Luenberger term in each observer is formulated as a linear matrix inequality problem, whereas the variable structure term is designed assuming uncertainty bounds. Simulation and experimental studies are included to demonstrate the performance of the proposed observers.

Index Terms—Electrochemical model, lithium-ion (Li-ion) batteries, nonlinear observer, single-particle model (SPM), state of charge (SOC).

I. INTRODUCTION

LITHIUM-ION (Li-ion) battery technology, the leading energy storage solution for various applications, is still suffering from the issues of safety, reliability, and high cost. To ensure safe and efficient operation, advanced battery management systems are required, which in turn rely on estimates of the state of charge (SOC) of each cell. There are several technical challenges to the accurate estimation of SOC. These challenges are mainly related to the scarcity of real-time measurements and parametric uncertainties [1], [2]. In this brief, we will focus on SOC estimation of an individual Li-ion battery cell and address these challenges by proposing observer designs based on uncertain electrochemical models.

The different techniques that have been proposed for SOC estimation in the literature can be broadly categorized into two categories: 1) open-loop model-based approaches such as coulomb counting and open circuit voltage (OCV) versus SOC map and 2) closed-loop model-based approaches. However, coulomb counting is susceptible to measurement inaccuracies and the OCV-SOC map technique is not realistic, as OCV is not measured in real time. Closed-loop model-based approaches can further

be divided into three categories depending on the type of the model used: 1) data-driven model-based approaches [3]; 2) equivalent circuit model (ECM)-based approaches [4], [5]; and 3) electrochemical model-based approaches. Although the data-driven and ECM-based approaches are simple in design and implementation, the drawbacks are extensive parameterization and lack of physical meaning of the model parameters.

Electrochemical model-based approaches, which are derived from principles of electrochemistry, are arguably more accurate than the other modeling approaches and they possess physical insight [6]. However, the complexity and computation burden of the full electrochemical model [known as pseudo-2D (P2D) model [7]] requires some level of model reduction for real-time implementable estimator designs. Some SOC estimation techniques have been proposed using this approach, including a residue grouping approach with a linear Kalman filter (KF) [8], particle filter (PF) [9], and a Luenberger type Partial Differential Equation (PDE) observer [10].

A particular reduction of the electrochemical model is known as the single-particle model (SPM), where the electrodes are approximated as spherical particles. A backstepping PDE estimator [1], an extended KF [11], [12], and an Unscented Kalman Filter [13] have been used for SPM-based SOC estimation. Some works proposed adaptive SOC estimation to take care of the parametric uncertainty using PF [14], adaptive PDE observer [15], and geometric observer [16]. The authors also proposed SPM-based nonlinear observer designs for SOC estimation [17] and adaptive sliding mode observer [18] for simultaneous SOC and parameter estimation.

The above review of the literature on electrochemical model-based SOC estimators revealed one or more of the following issues in existing approaches: 1) utilization of a fully linearized model; 2) being computationally expensive; and 3) lack of theoretical guarantees of the convergence of the estimator. In this brief, we address the above issues by extending [17], by: 1) including more details on modeling; 2) modifying the observer designs by adding a variable structure term for robustness and reestablishing the convergence conditions; and 3) providing experimental and additional simulation results.

This brief discusses two SPM-based observer designs consisting of a Luenberger term for the nominal model and a variable structure term for robustness to uncertainties. In each case, the design of the Luenberger term is cast as a linear matrix inequality (LMI) problem, whereas the variable structure term is designed by imposing bounds on the

Manuscript received October 12, 2014; accepted December 4, 2014. Manuscript received in final form December 10, 2014. This work was supported in part by the National Science Foundation under Grant CMMI-1055254 and in part by the U.S. Department of Energy through the Graduate Automotive Technology Education Program under Grant DE-EE0005571. Recommended by Associate Editor N. K. Kazantzis.

The authors are with the Clemson University International Center for Automotive Research, Greenville, SC 29607 USA (e-mail: satadrd@clemson.edu; beshah@clemson.edu; pisup@clemson.edu).

Color versions of one or more of the figures in this paper are available online at <http://ieeexplore.ieee.org>.

Digital Object Identifier 10.1109/TCST.2014.2382635

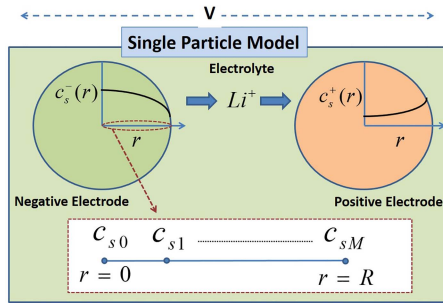


Fig. 1. Schematic of the SPM.

TABLE I
LI-ION BATTERY MODEL NOMENCLATURE

Symbol	Definition and Unit
A	Current collector area (m^2)
a_s^\pm	Specific surface area (m^2/m^3)
c_e	Electrolyte phase Li-ion concentration (mol/m^3)
c_s^\pm	Solid phase Li-ion concentration (mol/m^3)
$c_{s,e}^\pm$	Solid phase Li-ion concentration at surface (mol/m^3)
$c_{s,max}^\pm$	Solid phase Li-ion saturation concentration (mol/m^3)
D_s^\pm	Effective diffusion coefficient in solid phase (m^2/s)
F	Faraday's constant (C/mol)
I	Current (A)
L^\pm	Length of the electrodes (m)
r	Radial coordinate (cm)
R^\pm	Radius of solid active particle (m)
\bar{R}	Universal Gas Constant ($\text{J}/\text{mol}\cdot\text{K}$)
R_f	Contact film resistance (Ω)
T	Temperature (K)
U^\pm	Open circuit potential (V)
α^\pm	Charge transfer coefficient
ε_s^\pm	Active material volume fraction (dimensionless)
Superscript	
\pm	positive/negative electrode

uncertainty. Both observers offer simple designs and theoretically verifiable error convergence. The observers' performance is verified via simulations and experiments.

The rest of this brief is organized as follows. Section II reviews the Li-ion cell electrochemical model. Sections III and IV formulate the details of the observer designs. Sections V–VII present the simulation, experiments, and conclusion, respectively.

II. LITHIUM-ION CELL ELECTROCHEMICAL MODEL

A. Single-Particle Model (SPM)

The SPM is the reduced electrochemical model adopted for this brief. It is depicted by the schematic in Fig. 1 along with the nomenclature in Table I.

The SPM is obtained by approximating the electrodes as spherical particles along with volume-averaging assumptions [11], [12]. This approximation leads to two linear PDEs describing the material diffusion in two particles representing

each electrode. The PDEs and their boundary conditions are

$$\begin{aligned} \frac{\partial c_s^\pm}{\partial t} &= \frac{D_s^\pm}{r^2} \frac{\partial}{\partial r} \left(r^2 \frac{\partial c_s^\pm}{\partial r} \right) \\ \frac{\partial c_s^\pm}{\partial r} \Big|_{r=0} &= 0, \quad \frac{\partial c_s^\pm}{\partial r} \Big|_{r=R^\pm} = \frac{\pm I}{a_s^\pm F D_s^\pm A L^\pm} \end{aligned} \quad (1)$$

where c_s^\pm is the Li-ion concentration of the positive and negative electrode and I is the charge/discharge current. The specific surface area can be computed as $a_s^\pm = 3\varepsilon_s^\pm/R^\pm$. The output voltage map is derived using the Butler–Volmer kinetics, electrical potential, and electrode thermodynamic properties and is given by

$$\begin{aligned} V &= \frac{\bar{R}T}{\alpha^+ F} \sinh^{-1} \left(\frac{I}{2a_s^+ A L i_0^+} \right) - \frac{\bar{R}T}{\alpha^- F} \sinh^{-1} \left(\frac{I}{2a_s^- A L i_0^-} \right) \\ &\quad + U^+(c_{s,e}^+) - U^-(c_{s,e}^-) - R_f I \end{aligned} \quad (2)$$

where $c_{s,e}^+$ and $c_{s,e}^-$ are the surface concentrations of the positive and negative electrode, respectively; U^+ and U^- are the open circuit potentials of the positive and negative electrode, respectively; i_0^\pm are the exchange current densities given by

$$\begin{aligned} i_0^+ &= k_0^+ \sqrt{c_e c_{s,e}^+ (c_{s,max}^+ - c_{s,e}^+)} \\ i_0^- &= k_0^- \sqrt{c_e c_{s,e}^- (c_{s,max}^- - c_{s,e}^-)}. \end{aligned} \quad (3)$$

It is important to list some of the simplifying assumptions imbedded in the SPM. First, the mass and charge dynamics in the electrolyte are ignored. The charge in the solid material is also ignored and the molar flux is averaged. Next, the thermal effect is not considered. Moreover, the model may lose its predictive capability at higher currents. In the existing literature, there are some enhanced versions of the SPM applicable to higher charge–discharge rates. For example, the electrolyte concentration and potential dynamics are included in [19] using polynomial approximation functions to extend the applicability to higher charge–discharge rates. Similar types of models are presented in [20] along with consideration of nonuniform reaction distribution effects inside the electrode. In [21], an enhanced SPM with electrolyte diffusion and temperature-dependent parameters is presented. Despite these enhancements to the conventional SPM, in this brief, we shall work with the conventional form due to its suitability for the analytical nonlinear observer designs we propose. Then, to accommodate the limitations of the conventional SPM and parametric variations, we add uncertainty-handling capability in our observer designs.

B. Model Reduction and Finite-Dimensional Approximation

As the first step, we seek further reduction of the SPM, to improve the weak observability of the SPM states from differential voltage measurement [12]. We adopt the approach in [1], where the positive electrode Li-ion concentration is approximated as a function of the negative electrode Li-ion concentration assuming conservation of the number of Li-ions in the cell. This leads to observable forms for Li-concentration states when the negative electrode diffusion

PDE is discretized using the method of lines technique (based on finite central difference method). The spatial domain is discretized into $(M + 1)$ nodes, where $[c_{s0}, c_{s1}, \dots, c_{sM}]$ are the Li-ion concentration states at the nodes (Fig. 1), which leads to the following Ordinary Differential Equations:

$$\begin{aligned} \dot{c}_{s0} &= -3ac_{s0} + 3ac_{s1} \\ \dot{c}_{sm} &= \left(1 - \frac{1}{m}\right)ac_{s(m-1)} - 2ac_{sm} + \left(1 + \frac{1}{m}\right)ac_{s(m+1)} \\ \dot{c}_{sM} &= \left(1 - \frac{1}{M}\right)ac_{s(M-1)} - \left(1 - \frac{1}{M}\right)ac_{sM} - \left(1 + \frac{1}{M}\right)bI \end{aligned} \quad (4)$$

with $m = 1, \dots, (M - 1)$, discretization step $\Delta = R/M$, $a = D_s^-/\Delta^2$, and $b = 1/a_s^- F \Delta AL^-$. It is noted that the bulk SOC information can be computed using some combination of the states in (4), whereas c_{sM} indicates the surface SOC. The volume-averaged normalized bulk SOC can be computed from the SPM (1) using the following formula:

$$\text{SOC}_{\text{Bulk}} = \frac{1}{4\pi R^3 c_{s,\max}^-} \int_0^R 4\pi r^2 c_s^-(r, t) dr. \quad (5)$$

This formula can also be used on the discretized SPM in (4) to compute the bulk SOC of the cell as: $\text{SOC}_{\text{Bulk}} = \{(4\pi \Delta^3)/(4\pi R^3 c_{s,\max}^-)\} \sum_{j=1}^M j^2 c_{sj}$. The output voltage equation can be formed from (2) by substituting $c_{s,e}^- = c_{sM}$ and $c_{s,e}^+ = k_1 c_{sM} + k_2$, where k_1 and k_2 are constants in the algebraic relationship between the positive and negative electrode Li-ion concentration. Following the approach in [1], these constants can be derived considering the conservation of the total number of the Li-ions with $\partial/\partial t(n_{\text{Li}}) = 0$, where n_{Li} is the total number of Li-ions. Then, the positive electrode concentration can be computed as $c_{s,e}^+ = (1/\varepsilon_s^+ L^+ A)(-\varepsilon_s^- L^- A c_{sM} + n_{\text{Li}})$. Finally, the output voltage expression is given by

$$\begin{aligned} V &= \frac{\bar{R}T}{\alpha^+ F} \sinh^{-1}\left(\frac{I}{2a_s^+ AL^+ i_0^+}\right) - \frac{\bar{R}T}{\alpha^- F} \sinh^{-1}\left(\frac{I}{2a_s^- AL^- i_0^-}\right) \\ &+ U^+(k_1 c_{sM} + k_2) - U^-(c_{sM}) - R_f I \end{aligned} \quad (6)$$

where i_0^\pm are the exchange current densities given by

$$\begin{aligned} i_0^+ &= k_0^+ \sqrt{c_e(k_1 c_{sM} + k_2)(c_{s,\max}^+ - (k_1 c_{sM} + k_2))} \\ i_0^- &= k_0^- \sqrt{c_e c_{sM}(c_{s,\max}^- - c_{sM})}. \end{aligned} \quad (7)$$

III. STATE-SPACE MODEL FORMULATION AND ANALYSIS

The state-space model of the Li-ion cell can be written compactly in the following form:

$$\begin{aligned} \dot{x} &= Ax + Bu \\ y &= h(x, u) \end{aligned} \quad (8)$$

where states $x = [c_{s1}, \dots, c_{sM}]^T \in R^M$, input current $u = I \in R$, output voltage $y = V \in R$, the matrices A and B are derived from (4), and the output function h is formed by (6). The state-space model (8) represents a linear dynamics

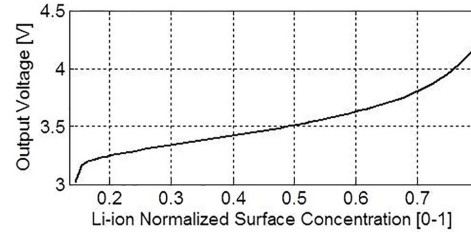


Fig. 2. Output voltage (y) as a function of state (x_M).

with a nonlinear output map. The estimation problem is to reconstruct the states of (8) using the output measurement.

Remark 1: Note that for the particular discretization adopted, the dynamics of the zeroth node (boundary node at $r = 0$) does not affect the state dynamics at the rest of the nodes, as can be observed in (4). This leads to unobservability of the state-space model when the equation for the zeroth node is included. However, by simply dropping this equation, we obtain an observable state-space model as given in (8). The observability of this nonlinear system has already been verified in [12]. If of interest, the zeroth node state could be approximated afterwards from the estimate of the state at the first node via an open-loop observer using the first equation in (4). The asymptotic convergence rate of the estimation error for the open-loop zeroth node observer will depend on the eigenvalue $(-3a)$ of the first equation in (4).

Remark 2: The output function h of the system is shown in Fig. 2 (with respect to x_M) for some given input. Given any input current u^* , the output function $h(x_M, u^*)$ retains the strictly increasing trend with respect to x_M . This has been verified by numerous offline simulation studies. It is also evident from Fig. 2 that the output function can be taken to be continuously differentiable with respect to the state within the operating region, which serves as a sufficient condition for Lipschitz continuity [22]. An estimate of the Lipschitz constant can be found as the $\max(\|\partial h/\partial x\|)$ within the operating region.

Remark 3: From the monotonicity observation above (or Fig. 2), we can infer that for any given $u = u^*$ and any two different points in the state-space $x_M^{(1)}$ and $x_M^{(2)}$, the following is always true:

$$\text{sgn}(h(x_M^{(1)}, u^*) - h(x_M^{(2)}, u^*)) = \text{sgn}(x_M^{(1)} - x_M^{(2)}). \quad (9)$$

Remark 4: To accommodate model (SPM) limitations and parametric uncertainties, we include unknown but bounded uncertainties in the nominal model (8) as follows:

$$\begin{aligned} \dot{x} &= Ax + Bu + \Delta_u(x, u) \\ y &= h(x, u) + \eta(x, u) \end{aligned} \quad (10)$$

where Δ_u and η represent state and/or input dependent uncertainties in state dynamics and the output, respectively.

IV. NONLINEAR OBSERVER DESIGNS

In this section, the details of the two observer designs are presented based on the uncertain model (10).

A. Observer Design I

In this first design, the observer structure is chosen as

$$\begin{aligned}\dot{\hat{x}} &= A\hat{x} + Bu + L_1(y - \hat{y}) + L_v \text{sgn}(y - \hat{y}) \\ \hat{y} &= h(\hat{x}, u)\end{aligned}\quad (11)$$

where $L_1 \in R^{M \times 1}$ is a constant gain representing the Luenberger term and $L_v \in R^{M \times 1}$ is a constant gain representing the variable structure term. Both gains have to be designed to ensure the convergence of the estimation error dynamics even in the presence of uncertainties. Subtracting (11) from (10), the estimation error dynamics of the observer can be written as

$$\dot{\tilde{x}} = A\tilde{x} + \Delta_u - L_1(\tilde{h} + \eta) - L_v \text{sgn}(\tilde{h} + \eta) \quad (12)$$

where $\tilde{x} = x - \hat{x}$ and $\tilde{h} = h(x, u) - h(\hat{x}, u)$.

To analyze the stability of the error dynamics, a Lyapunov function candidate $V = \tilde{x}^T P \tilde{x}$ is chosen, where P is an unknown positive definite symmetric matrix. The derivative of the Lyapunov function candidate is given as

$$\begin{aligned}\dot{V} &= \tilde{x}^T [A^T P + PA] \tilde{x} - \tilde{x}^T P (L_1 \tilde{h}) - (L_1 \tilde{h})^T P \tilde{x} \\ &\quad + 2\tilde{x}^T P (\Delta_u - L_1 \eta) - 2\tilde{x}^T P L_v \text{sgn}(\tilde{h} + \eta).\end{aligned}\quad (13)$$

Now, we separate \dot{V} into two parts: \dot{V}_1 involving the nominal error without uncertainty and \dot{V}_2 involving the uncertainty

$$\dot{V}_1 = \tilde{x}^T [A^T P + PA] \tilde{x} - \tilde{x}^T P (L_1 \tilde{h}) - (L_1 \tilde{h})^T P \tilde{x} \quad (14)$$

$$\dot{V}_2 = 2\tilde{x}^T P (\Delta_u - L_1 \eta) - 2\tilde{x}^T P L_v \text{sgn}(\tilde{h} + \eta). \quad (15)$$

Next, we investigate the negative definiteness of \dot{V}_1 and \dot{V}_2 , separately. Considering \dot{V}_1 first, to be negative definite, \dot{V}_1 needs to satisfy the following condition:

$$-\begin{bmatrix} \tilde{x}^T & z^T \end{bmatrix} \begin{bmatrix} A^T P + PA & -P \\ -P & 0 \end{bmatrix} \begin{bmatrix} \tilde{x} \\ z \end{bmatrix} > 0 \quad (16)$$

where $z = L_1 \tilde{h}$. The previously mentioned Lipschitz continuity condition (Remark 2) on the output function h can be written as

$$\|\tilde{h}\| \leq \gamma \|\tilde{x}\| \quad (17)$$

where γ is the Lipschitz's constant. We assume that (17) holds uniformly in u , and to determine γ , we impose boundedness on the input current u . Using Holder's inequality and Lipschitz continuity condition

$$\|z\| \leq \|L_1\| \|\tilde{h}\| \Rightarrow \|z\| \leq \gamma \|L_1\| \|\tilde{x}\| \Rightarrow z^T z \leq \gamma^2 L_1^T L_1 \tilde{x}^T \tilde{x}. \quad (18)$$

By adding a new (tuning) term, this condition can be modified as

$$z^T z - \tilde{x}^T [(\gamma^2 L_1^T L_1) I] \tilde{x} \leq -z^T M_1 z \quad (19)$$

where M_1 is some known positive definite matrix of the designer's choice and I is an identity matrix. Inequality (19) can be written as

$$\begin{bmatrix} \tilde{x}^T & z^T \end{bmatrix} \begin{bmatrix} (\gamma^2 L_1^T L_1) I & 0 \\ 0 & -I - M_1 \end{bmatrix} \begin{bmatrix} \tilde{x} \\ z \end{bmatrix} \geq 0. \quad (20)$$

Therefore, for the nominal dynamics of the system represented by \dot{V}_1 to converge to zero asymptotically, the following matrix inequalities must be satisfied for any suitable positive definite M_1 of the designer's choice:

$$\begin{aligned}P > 0, \quad & -\begin{bmatrix} A^T P + PA & -P \\ -P & 0 \end{bmatrix} > 0 \\ & \begin{bmatrix} (\gamma^2 L_1^T L_1) I & 0 \\ 0 & -I - M_1 \end{bmatrix} \geq 0.\end{aligned}\quad (21)$$

Using the s-procedure in [23], the second and third matrix inequalities of (21) lead to the condition

$$-\begin{bmatrix} A^T P + PA + (\tau \gamma^2 L_1^T L_1) I & -P \\ -P & -\tau(M_1 + I) \end{bmatrix} > 0 \quad (22)$$

with some multiplier coefficient $\tau \geq 0$. These matrix inequalities can be solved using MATLABs LMI Toolbox posing the problem in the following form:

$$\begin{bmatrix} A^T P + PA + Q & -P \\ -P & -SM_2 \end{bmatrix} < 0; \quad Q, S, P > 0 \quad (23)$$

where P is an unknown symmetric positive definite matrix, $Q = qI$ (with scalar $q = (\tau \gamma^2 L_1^T L_1)$) as the element along the diagonal) and $S = \tau I$ are unknown positive definite diagonal matrices with same elements along their diagonal, and $M_2 (= M_1 + I > I)$ is a positive definite matrix of the designer's choice. The feasible solution of this LMI problem will result in negative definite \dot{V}_1 , which guarantees asymptotic convergence of the estimation error for the nominal model. The unknown observer gain vector can be solved for from the following:

$$L_1^T L_1 = \frac{q}{\tau \gamma^2}. \quad (24)$$

The tuning mechanisms of this design procedure are the choice of M_2 and choice of individual observer gain vector elements based on the condition (24).

Next we consider \dot{V}_2 , which involves the uncertainties

$$\dot{V}_2 = 2\tilde{x}^T P (\Delta_u - L_1 \eta) - 2\tilde{x}^T P L_v \text{sgn}(\tilde{h} + \eta). \quad (25)$$

Under the condition $\|\tilde{h}\| \geq \|\eta\|$ (to be discussed below), the following is true:

$$\text{sgn}(\tilde{h} + \eta) = \text{sgn}(\tilde{h}). \quad (26)$$

Then, \dot{V}_2 can be written as

$$\begin{aligned}\dot{V}_2 &= 2\tilde{x}^T P (\Delta_u - L_1 \eta) - 2\tilde{x}^T P L_v \text{sgn}(\tilde{h}) \\ \Rightarrow \dot{V}_2 &= 2\tilde{x}^T P (\Delta_u - L_1 \eta) - 2\tilde{x}^T P L_v \frac{\tilde{h}}{\|\tilde{h}\|}.\end{aligned}\quad (27)$$

From Remark 3, the following can be written:

$$\text{sgn}(\tilde{h}) = \text{sgn}(\tilde{x}_M) \Rightarrow \frac{\tilde{h}}{\|\tilde{h}\|} = \frac{\tilde{x}_M}{\|\tilde{x}_M\|} = \frac{C\tilde{x}}{\|C\tilde{x}\|} \quad (28)$$

where $C = [0, \dots, 0, 1]$. Now we choose $L_v = KP^{-1}C^T$, where P comes from the solution of the LMI (23) and K is

TABLE II
SYSTEMATIC DESIGN PROCEDURE FOR OBSERVER I

Step 1: The choice of M_2 has to do with the feasibility of the LMI problem (23) and the desired convergence rate. Choose the structure $M_2 = \alpha I$. Initialize $\alpha > 1$.

Step 2: Increase α until a feasible LMI solution is achieved.

Step 3: Once the LMI is feasible, record the value of $L_1^T L_1$ and repeat the procedure with further increasing α . Record solution P as well.

Step 4: Finally, for all the feasible values of $L_1^T L_1$ assign the individual gain elements. Then select the observer gain L_1 that gives the desired convergence rate.

Step 5: Next, the variable structure gain parameter K can be chosen as follows:

$$K \geq \frac{\|\tilde{x}\|_{tol} \|P\| (\|\Delta_u\|_{max} + \|L_1\| \|\eta\|_{max})}{\|C\tilde{x}\|_{tol}}$$

where $\|\Delta_u\|_{max}$ and $\|\eta\|_{max}$ are assumed uncertainty bounds and $\|\tilde{x}\|_{tol}$ and $\|C\tilde{x}\|_{tol}$ are some tolerable steady-state error bounds.

a scalar parameter to be designed. Therefore, \dot{V}_2 becomes

$$\begin{aligned} \dot{V}_2 &= 2\tilde{x}^T P (\Delta_u - L_1 \eta) - 2\tilde{x}^T P L_v \frac{C\tilde{x}}{\|C\tilde{x}\|} \\ \Rightarrow \dot{V}_2 &= 2\tilde{x}^T P (\Delta_u - L_1 \eta) - 2K \tilde{x}^T P P^{-1} C^T \frac{C\tilde{x}}{\|C\tilde{x}\|} \\ \Rightarrow \dot{V}_2 &= 2\tilde{x}^T P (\Delta_u - L_1 \eta) - 2K \frac{(C\tilde{x})^T C\tilde{x}}{\|C\tilde{x}\|} \\ \Rightarrow \dot{V}_2 &\leq 2\|\tilde{x}\| \|P\| \|\Delta_u - L_1 \eta\| - 2K \|C\tilde{x}\|. \end{aligned} \quad (29)$$

Now, based on the selection of some high value of K , \dot{V}_2 will decrease as long as the following condition is satisfied:

$$K \geq \frac{\|\tilde{x}\| \|P\| \|\Delta_u - L_1 \eta\|}{\|C\tilde{x}\|}. \quad (30)$$

Therefore, from the overall analysis of \dot{V}_2 , it can be concluded that \dot{V}_2 will decrease until (26) or (30) is not satisfied. This leads to \tilde{x} settling on an error ball determined by the uncertainties and observer gains.

Now, consider the overall Lyapunov function derivative $\dot{V} = \dot{V}_1 + \dot{V}_2$. We have proved the asymptotic convergence of the nominal part to zero and convergence of the uncertain part to a certain error ball. Therefore, the estimation error will converge to a certain error ball in the presence of uncertainty. The systematic design procedure is summarized in Table II.

Note: An estimate of the values $\|\Delta_u\|_{max}$ and $\|\eta\|_{max}$ can be derived offline by comparing the open-loop SPM (*open-loop* indicates model without any measurement feedback in it) data with experimental or high-fidelity model (e.g., P2-D) data. For example, the two-norm of the error between averaged values of the states from the SPM and P2-D model can be recorded under different operating conditions and the maximum value of the two-norm multiplied by $\|A\|$ can be used as $\|\Delta_u\|_{max}$. A similar method can be applied to the voltage data and subsequently derive $\|\eta\|_{max}$. Similar approaches can be applied using experimental data of bulk SOC (from

accurate current measurement) and voltage. However, these estimates are conservative in nature and serve only as rough estimates.

B. Observer Design II

The drawback of a constant gain observer is that it will feed the output error with the same amplification throughout the state trajectory. In the state space, where the sensitivity of the output with respect to the states is very low (such as middle part of state region in Fig. 2), use of constant gain tends to inject noise/disturbance without any useful information. In this region, a constant gain could be disadvantageous. This fact motivates to have a gain-scheduled observer whose gain varies depending on the region of the state space. In this design, the output Jacobian is used to weigh the Luenberger gain leading to the following structure [24]:

$$\begin{aligned} \dot{\hat{x}} &= A\hat{x} + Bu + L_2 \left[\frac{\partial h}{\partial x} \right]_{x=\hat{x},u}^T (y - \hat{y}) + L_v \text{sgn}(y - \hat{y}) \\ \hat{y} &= h(\hat{x}, u) \end{aligned} \quad (31)$$

where $L_2 \in R^{M \times M}$ is the gain representing the Luenberger term and it is a constant weighted by the output Jacobian $[\partial h / \partial x] \in R^{1 \times M}$, and $L_v \in R^{M \times 1}$ is a constant gain representing the variable structure term.

Subtracting (31) from (10), the estimation error dynamics of the observer can be written as

$$\dot{\tilde{x}} = A\tilde{x} + \Delta_u - L_2 \left[\frac{\partial h}{\partial x} \right]_{x=\hat{x},u}^T (\tilde{h} + \eta) - L_v \text{sgn}(\tilde{h} + \eta) \quad (32)$$

where $\tilde{x} = x - \hat{x}$ and $\tilde{h} = h(x, u) - h(\hat{x}, u)$.

Again, a Lyapunov function candidate $V = \tilde{x}^T P \tilde{x}$ is chosen to analyze the convergence of the observer error dynamics, where P is an unknown positive definite symmetric matrix. The derivative of the Lyapunov function candidate is given as

$$\begin{aligned} \dot{V} &= \tilde{x}^T [A^T P + PA] \tilde{x} - 2\tilde{x}^T P L_2 \left[\frac{\partial h}{\partial x} \right]^T \tilde{h} \\ &\quad + 2\tilde{x}^T P \left(\Delta_u - L_2 \left[\frac{\partial h}{\partial x} \right]^T \eta \right) - 2\tilde{x}^T P L_v \text{sgn}(\tilde{h} + \eta). \end{aligned} \quad (33)$$

As before, we separate \dot{V} into two parts: \dot{V}_1 involving the nominal error without uncertainty and \dot{V}_2 involving the uncertainty

$$\dot{V}_1 = \tilde{x}^T [A^T P + PA] \tilde{x} - 2\tilde{x}^T P L_2 \left[\frac{\partial h}{\partial x} \right]^T \tilde{h} \quad (34)$$

$$\dot{V}_2 = 2\tilde{x}^T P \left(\Delta_u - L_2 \left[\frac{\partial h}{\partial x} \right]^T \eta \right) - 2\tilde{x}^T P L_v \text{sgn}(\tilde{h} + \eta). \quad (35)$$

Considering \dot{V}_1 first, the following condition is imposed to ensure the negative definiteness of the first term:

$$\tilde{x}^T [A^T P + PA] \tilde{x} \leq -\tilde{x}^T Q \tilde{x} - \tilde{x}^T P M_3 P \tilde{x} \quad (36)$$

where Q and M_3 are positive definite matrices of the designer's choice. The idea is to find a positive definite symmetric matrix P that satisfies (36). Assuming that such P exists, the estimator gain matrix is chosen as $L_2 = P^{-1}$.

TABLE III
SYSTEMATIC DESIGN PROCEDURE FOR OBSERVER II

Step 1: Similar to observer design I, the choice of Q and M_3 has to do with feasibility of the LMI problem (37) and the desired convergence rate. Choose the structure $Q = \varepsilon_1 I$ and $M_3 = \varepsilon_2 I$. Initialize $\varepsilon_1, \varepsilon_2 = 0$.

Step 2: Increase ε_1 and ε_2 until a feasible LMI solution is achieved.

Step 3: Once the LMI is feasible, record the gain L_2 and repeat the procedure with further increasing ε_1 and ε_2 . Record the solution P .

Step 4: Finally, from the set of feasible gains L_2 , select the one that gives the desired error convergence rate.

Step 5: Next, the variable structure gain parameter K can be selected in the same way as in Observer I.

This choice of estimator gain matrix makes the second term of (34) equal to $2\tilde{x}^T [\partial h / \partial x]^T \tilde{h}$. Now, consider the fact that h is a strictly increasing function of only the end state (x_{McSM}). This makes the x_M estimation error and output error sign always the same throughout the state trajectory (Remark 3). In addition, the Jacobian $\partial h / (\partial x_M)$ is always positive in the operating region. The second term on the right-hand side of (34) can be written as: $2[\tilde{x}_1, \dots, \tilde{x}_M][0, 0, \dots, (\partial h / \partial x_M)]^T \tilde{h} = 2\tilde{x}_M (\partial h / \partial x_M) \tilde{h}$. Now, $\tilde{x}_M \tilde{h} \geq 0$ at any point of the state space as the signs of \tilde{x}_M and \tilde{h} are always the same (Remark 3) and $\partial h / \partial x_M$ is always positive (Fig. 2). This leads to the fact that $2\tilde{x}^T [\partial h / \partial x]^T \tilde{h} \geq 0$ at any point of the state space. Now, it is clear that the first two terms in \dot{V}_1 are negative definite and the third term is negative semidefinite. This leads to a negative definite \dot{V}_1 , which is a sufficient condition for asymptotic convergence of the observer error for the nominal model. Therefore, the design of Luenberger observer boils down to finding a positive definite symmetric matrix P that satisfies (36). This can be cast as an LMI problem using Schur complements

$$\begin{bmatrix} A^T P + P A + Q & P \\ P & -M_3^{-1} \end{bmatrix} < 0; \quad P > 0. \quad (37)$$

Then the observer gain matrix can be obtained as $L_2 = P^{-1}$. The tuning mechanisms for this design are the choices of Q and M_3 .

The analysis and design for the uncertain part of the error dynamics represented by \dot{V}_2 is the same as that of *Observer Design I*. Considering the overall Lyapunov function derivative, we conclude that the estimation error will converge to a certain error ball in the presence of uncertainty. The systematic design procedure is given in Table III.

V. SIMULATION STUDIES

In this section, we present simulation results to demonstrate the effectiveness of the observers. For these simulation studies, the battery cell (metal-oxide positive electrode, graphite negative electrode, cell capacity 6 Ah) model parameters have been taken from [8]. We will show the

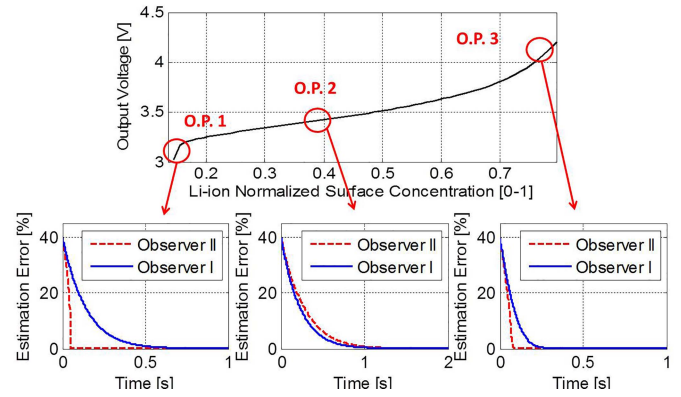


Fig. 3. Comparison of Observers I and II state estimation error convergence under 5C discharge. Temperature: 25 °C. Initial estimation error: 40%.

results in terms of normalized bulk concentration of Li-ions (bulk SOC) and output voltage estimation. A third-order model (discretizing the particle radius into four nodes) has been used. In Observer I, the Luenberger gain vector elements are chosen as $L^* = [0, 0, (L^T L)^{1/2}]^T$, where $(L^T L)^{1/2} = 0.1$. For Observer II, the Luenberger gain matrix is chosen as: $L_2^* = 0.07 * \text{ones}(3, 3)$.

First, the difference between Observers I and II is shown in Fig. 3 using SPM as plant model by showing their state estimation error at three different operating points. For illustration purposes, the same gains are used for Observers I and II so that they result in the same error convergence rate without weighing the Jacobian. Remember that Observer I uses the constant gain as it is, whereas Observer II has that gain weighted by the output Jacobian. In operating point 1 (OP 1) and operating point 3 (OP 3), Observer II has higher gain due to high sensitivity of the output Jacobian with respect to the state leading to faster convergence. In operating point 2 (OP 2), Observer II has lower gain due to low sensitivity of output Jacobian leading to slower convergence.

Fig. 4 shows the performance of the observers in the presence of uncertainty and initial condition error with the SPM as the plant. The variable structure gain parameter for both Observers I and II is chosen as $K = 0.01$. To emulate the uncertainty, we initialize the observers with the following parameter values: $D_{s,\text{observer}}^- = 100D_s^-$, $a_{s,\text{observer}}^- = 0.01a_s^-$, $R_{f,\text{observer}} = 0.5R_f$, and we add 5 mV noise in voltage measurement. As expected, even with the variable structure term, the estimation errors do not converge to zero due to output uncertainties.

Next, the performances of the observers are shown with a full-order P2-D model as the plant in Fig. 5. This illustration is provided to test the observers' capability in the presence of modeling uncertainties. The averaged normalized Li-ion concentration of the P2-D model's negative electrode is compared with the averaged Li-ion concentration from the observer and the steady-state error lies within 9%.

VI. EXPERIMENTAL RESULTS

In this section, we present results from experimental studies on the proposed observer designs applied to a commercial

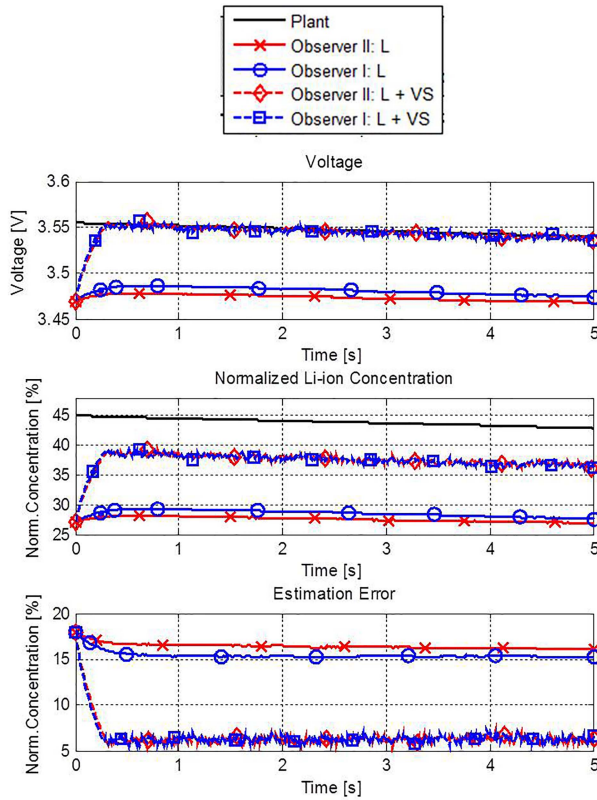


Fig. 4. Performance of the observers with and without the variable structure term in the presence of uncertainty in state dynamics and output channel. *L*: Luenberger term. *L* + *VS*: Luenberger and the variable structure term. Current profile: 8.3C discharge. Temperature: 25 °C. Initial SOC: 45%. Initial estimation error: 20%.

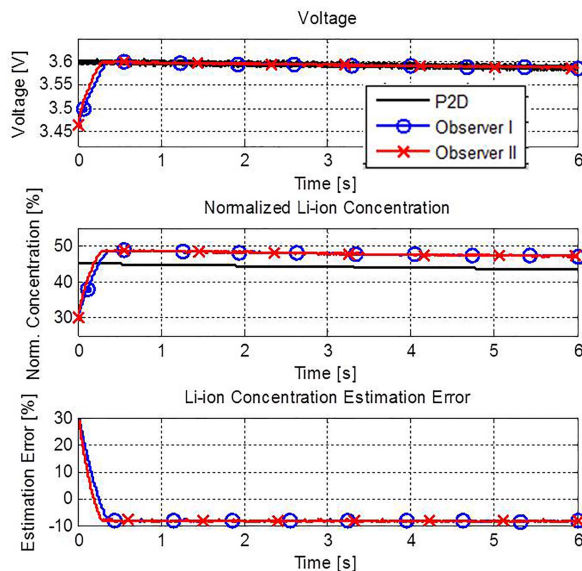


Fig. 5. Performance of the observers with P2-D model as the plant. Current profile: 5C discharge. Temperature: 25 °C. Initial SOC: 45%. Initial estimation error: 30%.

high-power LiFePO₄-graphite cell (capacity 2.3 Ah). First, some of the model parameters of (8) have been identified experimentally while others were adopted from available literature for this specific cell. To simplify the model to be fitted, we follow the assumption of constant exchange current

TABLE IV
MODEL PARAMETERS. *F* DENOTES FITTED VALUES

Parameters	Values
D_s^-	$5 \times 10^{-14} \text{ m}^2/\text{s}$ (F)
i_0^+	0.0016 A/m^2 (F)
i_0^-	0.2 A/m^2 (F)
R_f	0.222Ω (F)
k_1	-0.3944 (F)
k_2	20247 mol/m^3 (F)
a_s^-	$3.48 \times 10^5 \text{ m}^2/\text{m}^3$ [25]
ε_s^-	0.58 [26]
R^-	$5 \times 10^{-6} \text{ m}$ [25]
A	0.18 m^2 [25]
L^-	$3.4 \times 10^{-5} \text{ m}$ [25]
$c_{s,max}^+$	22806 mol/m^3 [27]
$c_{s,max}^-$	30555 mol/m^3 [28]

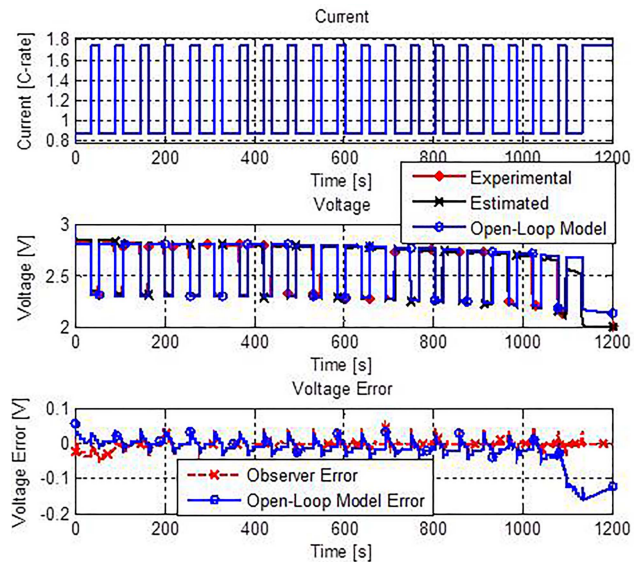


Fig. 6. Voltage response for pulse discharge test. Temperature: 25 °C. Initial SOC: 45%. Initial estimation error: 40%.

densities, as done in [25] and [26]. The following parameters are identified: D_s^- , i_0^+ , i_0^- , R_f , k_1 , and k_2 solving a nonlinear least square optimization problem. The values of the identified parameters are provided in Table IV. From the comparison of the open-loop model and the experimental data, the estimates of the variables $\|\Delta_u\|_{\max}$ and $\|\eta\|_{\max}$ are found as $2e-4$ and 0.15 , respectively. Here *open loop* indicates model without any measurement feedback in it.

To show the open-loop model validation and observer performance for SOC tracking, pulse discharge experiments are conducted. Observer II has been used for these experiments with both Luenberger and variable structure terms. To compute the actual bulk SOC of the cell, we used coulomb counting technique as in our experiments we have a high accuracy current measurement [10]. The results of the pulse discharge

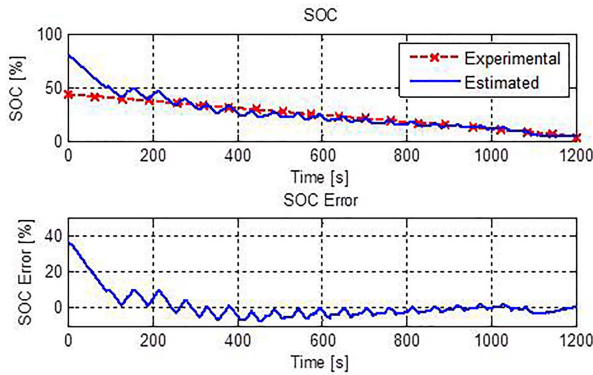


Fig. 7. SOC response for pulse discharge test. Temperature: 25 °C. Initial SOC: 45%. Initial estimation error: 40%.

test are shown in Figs. 6 (voltage response) and 7 (SOC response). Note that the open-loop model error in Fig. 6 is higher and shoots up toward the end, i.e., the low SOC region. However, the observer is able to overcome this uncertainty, producing more accurate voltage response. Note that there are visible spikes in the voltage errors which are due to the discontinuities in the voltage response owing to input discontinuities. As expected, the observer tracks the voltage with sufficient accuracy. The steady-state value of the SOC estimation error is within a 5% band.

VII. CONCLUSION

In this brief, two nonlinear robust observer designs have been presented for SOC estimation of Li-ion cells using an uncertain reduced electrochemical model given in the form of the SPM. The structure of both observers contains a Luenberger term for convergence of nominal error dynamics and a variable structure term to improve robustness toward model limitations/uncertainties. Simulation studies and experiments are presented to show the effectiveness of the observer designs.

However, there are some issues in the proposed designs that need further investigations. First, more experimental testing is needed especially with higher C -rates to completely validate the performance and limitations of the observers. In simulation studies, it is observed that the performance of the observers degrades for higher C -rates, especially in the presence of high output uncertainties. Second, thermal effects, which can play an important role particularly in a high-current scenario, are not included in the presented formulations. Finally, the variable structure term performs well in the presence of uncertainties in state dynamics while its performance is limited in the presence of output uncertainties.

REFERENCES

- [1] S. J. Moura, N. A. Chaturvedi, and M. Krstic, "PDE estimation techniques for advanced battery management systems—Part II: SOH identification," in *Proc. Amer. Control Conf. (ACC)*, 2012, pp. 566–571.
- [2] J. B. Siegel, X. Lin, A. G. Stefanopoulou, D. S. Hussey, D. L. Jacobson, and D. Gorsich, "Neutron imaging of lithium concentration in LFP pouch cell battery," *J. Electrochem. Soc.*, vol. 158, no. 5, pp. A523–A529, 2011.
- [3] B. Saha, K. Goebel, S. Poll, and J. Christophersen, "An integrated approach to battery health monitoring using Bayesian regression and state estimation," in *Proc. IEEE Autotestcon*, Sep. 2007, pp. 646–653.
- [4] G. L. Plett, "Extended Kalman filtering for battery management systems of LiPB-based HEV battery packs: Part 3. State and parameter estimation," *J. Power Sour.*, vol. 134, no. 2, pp. 277–292, 2004.
- [5] Y. Hu and S. Yurkovich, "Battery cell state-of-charge estimation using linear parameter varying system techniques," *J. Power Sour.*, vol. 198, pp. 338–350, Jan. 2012.
- [6] N. A. Chaturvedi, R. Klein, J. Christensen, J. Ahmed, and A. Kojic, "Algorithms for advanced battery-management systems," *IEEE Control Syst. Mag.*, vol. 30, no. 3, pp. 49–68, Jun. 2010.
- [7] M. Doyle, T. F. Fuller, and J. Newman, "Modeling of galvanostatic charge and discharge of the lithium/polymer/insertion cell," *J. Electrochem. Soc.*, vol. 140, no. 6, pp. 1526–1533, 1993.
- [8] K. A. Smith, C. D. Rahn, and C.-Y. Wang, "Model-based electrochemical estimation and constraint management for pulse operation of lithium ion batteries," *IEEE Trans. Control Syst. Technol.*, vol. 18, no. 3, pp. 654–663, May 2010.
- [9] M. F. Samadi, S. M. M. Alavi, and M. Saif, "An electrochemical model-based particle filter approach for lithium-ion battery estimation," in *Proc. IEEE 51st Annu. Conf. Decision Control (CDC)*, Dec. 2012, pp. 3074–3079.
- [10] R. Klein, N. A. Chaturvedi, J. Christensen, J. Ahmed, R. Findeisen, and A. Kojic, "Electrochemical model based observer design for a lithium-ion battery," *IEEE Trans. Control Syst. Technol.*, vol. 21, no. 2, pp. 289–301, Mar. 2013.
- [11] S. Santhanagopalan and R. E. White, "Online estimation of the state of charge of a lithium ion cell," *J. Power Sour.*, vol. 161, no. 2, pp. 1346–1355, 2006.
- [12] D. Di Domenico, A. Stefanopoulou, and G. Fiengo, "Lithium-ion battery state of charge and critical surface charge estimation using an electrochemical model-based extended Kalman filter," *ASME J. Dyn. Syst., Meas., Control*, vol. 132, no. 6, p. 061302, 2010.
- [13] S. Santhanagopalan and R. E. White, "State of charge estimation using an unscented filter for high power lithium ion cells," *Int. J. Energy Res.*, vol. 34, no. 2, pp. 152–163, 2010.
- [14] M. F. Samadi, S. M. M. Alavi, and M. Saif, "Online state and parameter estimation of the Li-ion battery in a Bayesian framework," in *Proc. Amer. Control Conf. (ACC)*, Jun. 2013, pp. 4693–4698.
- [15] S. J. Moura, N. A. Chaturvedi, and M. Krstic, "Adaptive PDE observer for battery SOC/SOH estimation via an electrochemical model," *ASME J. Dyn. Syst., Meas., Control*, vol. 136, no. 1, p. 011015, 2013.
- [16] Y. Wang, H. Fang, Z. Sahinoglu, T. Wada, and S. Hara, "Nonlinear adaptive estimation of the state of charge for lithium-ion batteries," in *Proc. 52nd IEEE Conf. Decision Control*, Dec. 2013, pp. 4405–4410.
- [17] S. Dey and B. Ayalew, "Nonlinear observer designs for state-of-charge estimation of lithium-ion batteries," in *Proc. Amer. Control Conf. (ACC)*, Jun. 2014, pp. 248–253.
- [18] S. Dey, B. Ayalew, and P. Pisu, "Combined estimation of state-of-charge and state-of-health of Li-ion battery cells using SMO on electrochemical model," in *Proc. 13th Int. Workshop Variable Struct. Syst.*, 2014, pp. 1–6.
- [19] S. K. Rahimian, S. Rayman, and R. E. White, "Extension of physics-based single particle model for higher charge–discharge rates," *J. Power Sour.*, vol. 224, pp. 180–194, Feb. 2013.
- [20] W. Luo, C. Lyu, L. Wang, and L. Zhang, "A new extension of physics-based single particle model for higher charge–discharge rates," *J. Power Sour.*, vol. 241, pp. 295–310, Nov. 2013.
- [21] T. R. Tanim, C. D. Rahn, and C.-Y. Wang, "A temperature dependent, single particle, lithium ion cell model including electrolyte diffusion," *J. Dyn. Syst., Meas., Control*, vol. 137, no. 1, p. 011005, 2014.
- [22] H. J. Márquez, *Nonlinear Control Systems: Analysis and Design*. New York, NY, USA: Wiley, 2003.
- [23] S. Boyd, L. El Ghaoui, E. Feron, and V. Balakrishnan, *Linear Matrix Inequalities in System and Control Theory*, vol. 15. Philadelphia, PA, USA: SIAM, 1994.
- [24] A. Johansson, and A. Medvedev, "An observer for systems with nonlinear output map," *Automatica*, vol. 39, no. 5, pp. 909–918, 2003.
- [25] E. Prada, D. Di Domenico, Y. Creff, J. Bernard, V. Sauvart-Moynot, and F. Huet, "Simplified electrochemical and thermal model of LiFePO₄-graphite Li-ion batteries for fast charge applications," *J. Electrochem. Soc.*, vol. 159, no. 9, pp. A1508–A1519, 2012.
- [26] K. Smith and C.-Y. Wang, "Power and thermal characterization of a lithium-ion battery pack for hybrid-electric vehicles," *J. Power Sour.*, vol. 160, no. 1, pp. 662–673, 2006.
- [27] C. Delacourt and M. Safari, "Analysis of lithium deinsertion/insertion in LiyFePO₄ with a simple mathematical model," *Electrochim. Acta*, vol. 56, no. 14, pp. 5222–5229, 2011.
- [28] S. Santhanagopalan, Q. Guo, P. Ramadass, and R. E. White, "Review of models for predicting the cycling performance of lithium ion batteries," *J. Power Sour.*, vol. 156, no. 2, pp. 620–628, 2006.